Published in final edited form as:
Inorg Chem. 2009 October 5; 48(19): 9155–9165. doi:10.1021/ic9008784.

DFT Calculations on Mössbauer Parameters of Nonheme Iron Nitrosyls

Kathrin H. Hopmann[a], **Abhik Ghosh**[*,a], and **Louis Noodleman**[*,b]

[a] Center for Theoretical and Computational Chemistry and Department of Chemistry, University of Tromsø, N-9037 Tromsø. Norway

[b] Department of Molecular Biology, TPC15, The Scripps Research Institute, 10550 N. Torrey Pines Road, La Jolla, CA 92037, USA

Abstract

DFT calculations on transition metal nitrosyls often reveal unusual spin density profiles, involving substantial spatial separation of majority and minority spin densities. Against this context, there is a significant lack of studies where DFT calculations have been quantitatively calibrated against experimental spectroscopic properties. Reported herein are DFT calculations of Mössbauer isomer shifts and quadrupole splittings for 21 nonheme iron complexes (26 distinct iron sites) including 9 iron nitrosyls. Low- (S = 1/2) and high-spin (S = 3/2) $\{FeNO\}^7$ complexes, S = 1/2 $\{Fe(NO)_2\}^9$ species, and polynuclear iron nitrosyls are all represented within the set of compounds examined. The general conclusion with respect to isomer shifts is that DFT (OLYP/STO-TZP) performs comparably well for iron nitrosyls and for iron complexes in general. However, quadrupole splittings are less accurately reproduced for nitrosyl complexes.

Keywords

DFT; Mössbauer; iron; nitrosyl; broken-symmetry

Introduction

The subtlety and diversity of metal-nitrosyl bonding has long fascinated inorganic and theoretical chemists alike. The discovery of NO's ubiquitous roles in biology, along with the potential importance of NO donors as blood pressure-controlling and anticancer drugs, has continued to fuel this fascination.[1,2,3,4,5] Density functional theory (DFT) has proved to be an invaluable tool in chemists' attempts to deepen their understanding of metal-NO bonding and a great deal of progress has been made.[6] Open questions remain, however. One such question concerns how well DFT, or more precisely a given functional, performs in describing a metal-NO linkage, compared with experiment.

An intriguing aspect of DFT studies on transition metal nitrosyls concerns their spin densities, which very often exhibit broken-symmetry character, i.e. a significant spatial separation of majority and minority spin densities.[7,8,9,10,11] There is no reason to doubt the qualitative correctness of such a description. Nevertheless, there have been few detailed studies calibrating DFT-derived electron densities against experimental spectroscopic parameters. We have

*corresponding author: lou@scripps.edu, abhik.ghosh@uit.no.

Supporting Material
Optimized coordinates (OLYP, COSMO) for all complexes.

attempted such a calibration here, via DFT calculations of Mössbauer isomer shifts and quadrupole splittings for a set of 9 nonheme iron nitrosyls, as well as for a similar number of nonnitrosyl iron complexes. Our study encompasses a fairly diverse set of iron nitrosyls – low- (S = 1/2) and high-spin (S = 3/2) $\{FeNO\}^7$ complexes, $\{Fe(NO)_2\}^9$ species, and polynuclear complexes including the anion of Roussin's Black Salt. The superscripted number n in $\{FeNO\}^n$ or $\{Fe(NO)_2\}^n$ refers to the Enemark-Feltham electron count[12], which is the number of *d* electrons plus the number of electrons in NO π* orbitals. This notation neatly avoids the sometimes contentious issue of the degree of charge transfer between the metal and NO units.

A number of DFT studies of Mössbauer isomer shifts and quadrupole splittings have been reported in the literature,[13,14,15,16,17,18] including computations on heme-nitrosyls[19,20] and nonheme iron nitrosyl complexes.[10,21,22,23] The agreement with experimental Mössbauer data (isomer shifts and quadrupole splittings) in these studies is generally good, although some dependence on the exchange-correlation functional has been observed.[16] Evaluation of the performance of different DFT functionals for computing isomer shifts of 20 iron complexes (including 2 nonheme FeNO complexes) indicated that hybrid functionals performed slightly better than pure DFT functionals.[24,25] Here we have used OLYP (and B3LYP) to evaluate the performance of DFT for computing Mössbauer parameters of a diverse set of nonheme iron nitrosyls.

Computational Details

Geometry optimizations were performed with the OLYP[26,27] functional and all-electron Slater-type triple-ζ plus polarization (STO-TZP) basis sets, as implemented in the Amsterdam Density Functional (ADF) 2007 program package.[28] Solvent effects were modelled with the COnductor-like Screening MOdel (COSMO)[29], employing methanol as the solvent (radius = 2.53, dielectric constant = 32.6). All initial geometries (except for $[Fe(H_2O)_5(NO)]^{2+}$) were obtained from crystallographic coordinates and were optimized both in gas phase and with COSMO. For overall S = 0, antiferromagnetically coupled systems, Noodleman's[30] method was employed for computing the broken-symmetry states. This method involves a self-consistent field (SCF) calculation of the high-spin (i.e. ferromagnetically coupled) state of a given complex, followed by flipping of the spin on selected atoms to result in an antiferromagnetically coupled state. The spin-flipped electronic structure is then used as starting guess for geometry optimization of the broken-symmetry state. The spin densities of the broken symmetry states were visualized with Chemcraft.[31]

ADF, in conjunction with the hyper2003 program,[32] was used to calculate Mössbauer parameters. Electric field gradients calculated with ADF (OLYP[26,27] and B3LYP[27,33]) were used to calculate quadrupole splittings with our QUTIL code. Nuclear electron densities were computed with hyper2003 (using the short hypers2003 version), based all-electron single-point calculations with ADF. Unrestricted Corresponding Orbitals[34] (UCOs) were analyzed with ORCA[35] single point calculations (OLYP or B3LYP in combination with the TZVP basis set[36]) on geometries optimized with ADF (OLYP, COSMO). This analysis involves a unitary transformation of the α and β orbitals to create orbital pairs with maximum overlap. An overlap of 1 is consistent with a covalent interaction, whereas orbital pairs with overlaps significantly lower than 1 are considered magnetic orbitals. Singly occupied orbitals (SOMOs) lack an orbital partner and thus have zero overlap.[34] The UCOs were visualized with gOpenMol.[37]

The Heisenberg coupling constants, *J*, refer to the $H = -2JS_AS_B$ spin Hamiltonian and were computed at the optimized, broken-symmetry OLYP/COSMO geometries (ADF) with either ORCA or ADF. Both the Noodleman formalism[38] (HS = high-spin, BS = broken symmetry),

$$J = -(E_{HS} - E_{BS})/4S_A S_B \quad (1)$$

and the Yamaguchi formalism,39

$$J = -(E_{HS} - E_{BS})/(\langle S^2\rangle_{HS} - \langle S^2\rangle_{BS}) \quad (2)$$

were used to calculate the Heisenberg *J*'s.

Results and Discussion

The complexes studied

Broken-symmetry calculations were performed on an electronically diverse set of mononuclear and polynuclear compounds, including 9 iron nitrosyl complexes (Scheme 1) and 12 nonnitrosyl iron complexes (Table 1).

The twelve nonnitrosyl compounds studied are all iron-sulfur complexes. The three open-shell, mononuclear complexes studied, $[Fe(SEt)_4]^-$ (S = 5/2) and the two S = 2 Fe^{2+} complexes $[Fe(S_4C_8O_4)]^{2-}$ and $[Fe(SPh)_4]^{2-}$, may be regarded as synthetic analogues of the oxidized and the reduced forms of the $[Fe(SR)_4]$ center of bacterial rubredoxins.[40,41,42] The three antiferromagnetically coupled diferric complexes $[Fe_2S_2(S_2\text{-}o\text{-}xyl)_2]^{2-}$,[43,44,45] $[Fe_2S_2(OPh\text{-}p\text{-}CH_3)_4]^{2-}$,[45] and $[Fe_2S_2(C_4H_4N)_4]^{2-}$,[45] were originally prepared as models for plant-type 2Fe-2S ferredoxins and Rieske proteins.[45,46,47] The irons in these binuclear complexes are linked by sulfide bridges, but in addition have different oxygen, nitrogen or sulfur ligands. The six 4Fe-4S complexes $[Fe_4S_4(SPh)_4]^{2-}$,[48,51] $[Fe_4S_4(OPh)_4]^{2-}$,[49] $[Fe_4S_4(SPh)_2Cl_2]^{2-}$,[51] $[Fe_4S_4(OPh)_2Cl_2]^{2-}$,[51] $[Fe_4S_4Cl_4]^{2-}$,[50,51] and $[Fe_4S_4(SCH_2CO_2Et)_4]^{2-}$52 may be viewed as models of the 4Fe-4S cubane centers in ferredoxins and high-potential iron proteins (HiPIPs). Antiferromagnetic coupling between pairs of irons in these tetramers leads to overall diamagnetic compounds. Each iron pair, however, may be envisioned as originating from Fe^{2+} ferromagnetically coupled to Fe^{3+}. Delocalization of a "minority-spin" electron within the pair results in an average iron oxidation state of +2.5 (Table 1).

The nine iron nitrosyls included in this study are all $\{FeNO\}^7$ and/or $\{Fe(NO)_2\}^9$ species (Scheme 1). Two mononuclear, paramagnetic $\{FeNO\}^7$ complexes have been studied: $[Fe(H_2O)_5(NO)]^{2+}$ (S = 3/2), which is known from the classic brown ring test for nitrate,[53] and the dithiocarbamate complex $[Fe(NO)(dtc\textit{i}\text{-}Pr_2)_2]$ (S = 1/2) (Scheme 1, **A** and **B**).[54,55] Also included are two mononuclear S = 1/2 $\{Fe(NO)_2\}^9$ complexes, $[Fe(SC_2H_3N_3)(SC_2H_2N_3)(NO)_2]$ (Scheme 1, **D**), which has two 1,2,4-triazole-3-thionyl ligands,[56,57] and $[Fe(SPh)_2(NO)_2]^-$ (Scheme 1, **C**), which is a synthetic analogue of the dinitrosyl iron complexes (DNICs) formed from the reaction of 4Fe-4S proteins with NO.[58] Two binuclear NO complexes have been studied: the diamagnetic bis-$\{FeNO\}^7$ complex $[Fe_2(NO)_2(Et\text{-}HPTB)(O_2CPh)]^{2+}$ (Et-HPTB = *N*, *N*, *N*′, *N*′-tetrakis-(*N*-ethyl-2-benzimidazolylmethyl)-2-hydroxy-1,3-diaminopropane) (Scheme 1, **E**),[59] and the paramagnetic, S = 1, thiolate-bridged $\{FeNO\}^7$-$\{Fe(NO)_2\}^9$ complex $[Fe(NO)_2\{Fe(NO)(N(CH_2CH_2S)_3)\}\text{-}S, S']$ (Scheme 1, **F**).[60,61] The neutral $[Fe_4(NO)_4(\mu_3\text{-}S)_4]$ complex has the same cubane core as the 4Fe-4S complexes mentioned above, but all four iron centers are $\{FeNO\}^7$ units (Scheme 1, **H**).[62,63,64] The reduced form of this complex, $[Fe_4(NO)_4(\mu_3\text{-}S)_4]^-$, was also studied.[64] The tetranuclear $[Fe_4(NO)_7(\mu_3\text{-}S)_3]^-$ species (Scheme 1G), known as Roussin's black salt (RBS),[63,65,66] was not included in the isomer shift fit but was chosen instead as a test of the fitted parameters.

(b) Basic Description of the Broken Symmetry States

The nonnitrosyl complexes feature iron oxidation states of Fe^{2+}, $Fe^{2.5+}$ or Fe^{3+} and exhibit OLYP iron spin populations (absolute values) of 3.1 to 3.8 (Table 1), which is typical for DFT calculations on divalent and trivalent high-spin iron complexes. The iron spin population of the high-spin Fe^{3+} complex $[Fe(SEt)_4]^-$ is only slightly higher than that of the mononuclear S = 2 Fe^{2+} complexes $[Fe(S_4C_8O_4)]^{2-}$ and $[Fe(SPh)_4]^{2-}$ (Table 1). The binuclear complexes $[Fe_2S_2(S_2\text{-}o\text{-xyl})_2]^{2-}$, $[Fe_2S_2(OPh\text{-}p\text{-}CH_3)_4]^{2-}$, and $[Fe_2S_2(C_4H_4N)_4]^{2-}$ feature antiferromagnetically coupled, high-spin Fe^{3+} centers, with Fe spin populations (absolute values) of 3.5–3.7 for the broken-symmetry states (Table 1). As alluded to above, the broken-symmetry states of the six $[Fe_4S_4L_4]^{2-}$ complexes studied exhibit antiferromagnetic coupling between two delocalized, ferromagnetically coupled Fe^{2+}-Fe^{3+} pairs (Table 1). The Fe spin populations in these complexes are all in the range 3.26 ± 0.10 (Table 1).

The spin density profiles, MO occupancies and Mössbauer parameters of the iron nitrosyl complexes studied are indicative of high-spin iron centers, except for $[Fe(NO)(dtc\textit{i}\text{-}Pr_2)_2$. The experimentally determined isomer shifts for these complexes are in the range 0.2–0.8 (see below), which agrees best with a high-spin Fe^{2+} or Fe^{3+} assignment.[67] The OLYP Fe spin populations vary considerably across the NO complexes, with the absolute values ranging from 0.6–3.5 (Table 2). The NO ligands exhibit oppositely aligned spin populations of 0.2–0.9 (Table 2), relative to the iron centers to which they are attached. The low Fe and NO spin populations in some of the iron nitrosyls reflect strong antiferromagnetic coupling within and between FeNO units, which results in partial cancellation of spin density, as discussed further below.

The linear $\{FeNO\}^7$ unit of S = 3/2 $[Fe(H_2O)_5(NO)]^{2+}$ (Figure 1, **A**) exhibits OLYP spin populations of 3.55 on Fe and −0.81 on NO (Table 2). The cylindrically symmetric minority spin density on the NO supports a high-spin Fe^{3+} NO^- formulation, apparently consistent with Mössbauer, EPR spectroscopic and kinetics results.[53] In contrast, the OLYP spin density of the S = 1/2 $\{FeNO\}^7$ complex $[Fe(NO)(dtc\textit{i}\text{-}Pr_2)_2]$ suggests an intermediate-spin Fe^{3+} center (S = 3/2) coupled to an NO^- (S = 1) (Figure 1, **B**).[68] In the same vein, S = 1/2 $\{Fe(NO)_2\}^9$ units may be described either as high-spin Fe^{3+} (S = 5/2) antiferromagnetically coupled to two NO^- (S = 1) diradicals or as high-spin Fe^{1+} (S = 3/2) antiferromagnetically coupled to two $NO^\bullet$ radicals. The OLYP spin populations for $[Fe(SPh)_2(NO)_2]^-$ and $[Fe(SC_2H_3N_3)(SC_2H_2N_3)(NO)_2]$ (Figure 1, **C** and **D**) are similar, 1.57 and 1.75, respectively, on iron, and −0.44 and −0.50, respectively, on each NO (Table 2).

The binuclear complex $[Fe(NO)_2\{Fe(NO)(N(CH_2CH_2S)_3)\}\text{-}S, S']$ (Figure 1, **F**; Table 2) may be viewed as an S = 3/2 $\{FeNO\}^7$ unit and an S = 1/2 $\{Fe(NO)_2\}^9$ unit, coupling antiferromagnetically to yield an overall S = 1 ground state. The Fe spin population of the $\{FeNO\}^7$ unit is 2.61, which is lower than that in $[Fe(H_2O)_5(NO)]^{2+}$ (3.55, Table 2), indicating partial cancellation of spin density due to strong antiferromagnetic coupling with the$\{Fe(NO)_2\}^9$ unit. Analysis of the magnetic orbitals confirms this picture (see below). The antiferromagnetic iron complex $[Fe_2(NO)_2(Et\text{-}HPTB)(O_2CPh)]^{2+}$ (Figure 1, **E**) consists of a pair of oppositely aligned, S = 3/2$\{FeNO\}^7$ units, each with an Fe spin populations of ±3.47 (Table 2). The antiferromagnetic coupling between the iron centers is weak due to the nature of the bridging atoms (the experimental coupling constant is only $J = -23\ cm^{-1}$)[59] and it has little effect on the Fe spin population.

The broken-symmetry spin density for the RBS anion $[Fe_4(NO)_7(\mu_3\text{-}S)_3]^-$ suggests a high-spin Fe^{3+} NO^- description for the apical FeNO group (Figure 1, **G**). The OLYP spin populations are −1.18 on the apical $\{FeNO\}^7$ iron and 0.62 on each of the $\{Fe(NO)_2\}^9$ irons (Table 2). The Fe spin populations (±1.21) for the broken-symmetry state of the $[Fe_4(NO)_4(\mu_3\text{-}S)_4]$ are similar to those in RBS (apical Fe site, Table 2). The $\{FeNO\}^7$ units in this complex couple pairwise, giving an overall S = 0 state (Figure 1, **I**, Table 2). For the reduced form of this complex,

$[Fe_4(NO)_4(\mu_3\text{-}S)_4]^-$, two different $M_S = 1/2$ broken-symmetry states of comparable energy were found. One of the states features aligned spin populations (1.13 to 1.16) on three of the iron centers and oppositely aligned spin density (−2.17) on the fourth iron. In the other broken-symmetry state, the iron atoms are pairwise identical, with symmetry-distinct Fe spin populations of +1.94 and −1.29 (Table 2; Figure 1, **H**). This state, which may be described as a pair of effectively $\{FeNO\}^{7.5}$ centers antiferromagnetically coupled to a pair of $\{FeNO\}^7$ centers, was chosen for computing Mössbauer parameters.

(c) UCO Analysis

All polynuclear complexes included in our study exhibit antiferromagnetic coupling between the metal centers (Table 1, Figure 1). The iron nitrosyl complexes, in addition, feature antiferromagnetic coupling between iron and NO (Table 2). The magnetic orbital pairs involved in the spin coupling have been analyzed here by computing the unrestricted corresponding orbitals (UCOs).[34,69,70] The overlap between corresponding α and β orbitals is related to the strength of the antiferromagnetic coupling, which has also been quantified here by computing the Heisenberg coupling constants *(J)*. The magnetic coupling has been analyzed in three complexes, a binuclear iron complex without nitrosyl ligands, a mononuclear iron nitrosyl, and a binuclear iron nitrosyl.

UCO analysis of the binuclear complex $[Fe_2S_2(S_2\text{-o-xyl})_2]^{2-}$ revealed 5 magnetic orbital pairs mainly centered on iron (Figure 2). OLYP calculations gave overlap values of 0.100, 0.116, 0.311, 0.470, and 0.623 for the 5 orbital pairs. With B3LYP, smaller overlap values were obtained, 0.051, 0.110, 0.207, 0.355, and 0.465, respectively. The number of UCOs is consistent with antiferromagnetic coupling between two S = 5/2 Fe^{3+} centers. The experimentally determined Heisenberg *J* of $-148\ cm^{-1}$ ($H = -2JS_AS_B$)[44] compares well with the B3LYP (ORCA) value of $-227\ cm^{-1}$ obtained with equation (1) ($S_A = S_B = 5/2$) and of $-223\ cm^{-1}$ obtained with equation (2). OLYP (ORCA) gave somewhat larger coupling constants of −309 and $-301\ cm^{-1}$, respectively.

As mentioned above, the spin density of $[Fe(H_2O)_5(NO)]^{2+}$ is best described as arising from a high-spin Fe^{3+} center antiferromagnetically coupled to an NO^- diradical.[53] UCO analysis revealed three 3 SOMOs mainly centered on iron and two pairs of Fe(d_π)-NO(π^*)-based magnetic orbitals (Figure 3). With OLYP, the overlap values are 0.847 and 0.852, whereas with B3LYP, they are slightly lower, 0.786 and 0.797, respectively. The antiferromagnetic coupling in $[Fe(H_2O)_5(NO)]^{2+}$ thus involves two Fe d_π electrons and the two NO π^* electrons, in agreement with the above description.[53] OLYP/COSMO (ADF) calculations gave a Heisenberg *J* of $-3321\ cm^{-1}$ with equation (1) ($S_A = 5/2$, $S_B = 1$) and $-2898\ cm^{-1}$ with equation (2). The exact values of these coupling constants are clearly not particularly significant, except that they reflect the great strength of the antiferromagnetic coupling.

UCO analysis of $[Fe(NO)_2\{Fe(NO)(NS_3)\}\text{-}S, S']$ revealed two SOMOs largely localized on the $\{FeNO\}^7$ unit (OLYP, Figure 4, B and C). The antiferromagnetic coupling between the iron centers is described primarily by a pair of magnetic orbitals with an overlap of 0.662 (OLYP, Figure 4, A). However, there are 6 orbital pairs for which the overlap deviates mildly from unity, including two located on the $\{FeNO\}^7$ unit (OLYP overlaps 0.928 and 0.959) and four located on the $\{Fe(NO)_2\}^9$ unit (OLYP overlaps 0.970, 0.979, 0.981, and 0.984). With OLYP/COSMO (ADF), the Heisenberg *J* between the $\{FeNO\}^7$ ($S_A = 3/2$) and $\{Fe(NO)_2\}^9$ ($S_B = 1/2$) units turned out to be $-1455\ cm^{-1}$ with equation (1) and $-1243\ cm^{-1}$ with equation (2), which is indicative of remarkably strong antiferromagnetic coupling. This coupling is far stronger than that in the binuclear nonnitrosyl complex mentioned above. The strong coupling also accounts for the low spin densities, especially Fe spin populations, found for the $[Fe(NO)_2\{Fe(NO)(NS_3)\}\text{-}S, S']$ complex.

(d) Isomer Shift Calculations

The Mössbauer isomer shift (δ) arises from the interaction of the iron nucleus with the *s*-electron density. This interaction affects the nuclear energy levels, resulting in a shift of the spectrum compared to a reference. Experimentally, δ is typically determined relative to α-iron at room temperature. The isomer shift for a given iron center cannot be computed directly, but it may be predicted from a correlation between known isomer shifts and computed nuclear electron densities for a set of iron complexes. Here we have prepared such a fit based on the iron compounds in Table 1 (excluding $[Fe_4(NO)_7(\mu_3\text{-}S)_3]^-$). The electron density at the nucleus of each iron center was computed with hyper2003 on the basis of a single-point calculation with ADF. Linear regression is performed by employing the formula:

$$\delta=\alpha[\rho(0) - A]+C \quad (3)$$

where δ (in mms^{-1}) is the isomer shift, ρ(0) (in ea_0^{-3}) the electron density at the nucleus, α (in $e^{-1}a_0^3mms^{-1}$) the slope, and C (in mms^{-1}) the intercept (a_0 = bohr radius = 0.529 Å). The constant A (ea_0^{-3}), which is similar to the electron density at the iron nucleus in the reference state, has been introduced into equation (3) to ensure that [ρ(0)–A] corresponds to a small value, thereby facilitating accurate linear regression. This is necessary because ρ(0) is large (around 11877), whereas the variation in the nuclear electron density between iron atoms in different environments is small, between 0 to 2. A value of A = 11877 was employed here.

Mössbauer parameters are temperature dependent; an increase in temperature will result in a lower isomer shift. Most Mössbauer spectra are recorded at 4.2 K (liquid helium), and for the fit reported here, experimental isomer shifts obtained at higher temperatures are corrected to the value expected at 4.2 K by taking into account the second-order Doppler shift. Here we have corrected the isomer shift by assuming a linear correction of 0.12 mms^{-1} for a temperature decrease from 300 to 4.2 K. The same correction was also applied in earlier isomer shift fits.[14]

For complexes with nonequivalent iron centers, the individual isomer shifts can sometimes be determined from the experimental Mössbauer spectrum. However, in many cases, the experimental data are translated into a single isomer shift. For complexes with only one reported isomer shift, the experimental value has been considered to be an average over the different iron centers and has been plotted against the average of the computed Fe nuclear electron densities. One exception is $[Fe_4(NO)_4(\mu_3\text{-}S)_4]^-$, whose nonequivalent $\{FeNO\}^7$ and $\{FeNO\}^{7.5}$ centers have been treated separately. For two of the Fe_4S_4 complexes, $[Fe_4S_4(SPh)_2Cl_2]^{2-}$ and $[Fe_4S_4(OPh)_2Cl_2]^{2-}$, two isomer shifts (and two quadrupole splittings) were obtained from the experimental Mössbauer spectrum,[51] most likely corresponding to the Fe-Cl and the Fe-(O/S)Ph centers. As it was not obvious which isomer shift belongs to which center, they were assigned based on the expectation that the higher computed nuclear density should correspond to the smaller isomer shift.

The final “universal fit” included 20 iron complexes (24 distinct iron sites, Figure 5). The r^2 value computed for the fit involving solvent-optimized complexes is 0.915, while α and C are −0.315 and 0.432, respectively (Table 3). For optimizations in gas phase, r^2 = 0.911, α = −0.300 and C = 0.416 (Table 3). The parameters obtained from gas-phase and solvent calculations are thus very similar. A previous OLYP-based fit (ADF, TZP) yielded fit parameters similar to those obtained here.[14] Thus, a fit including mononuclear and binuclear complexes with $Fe^{2.5+}$, Fe^{3+}, $Fe^{3.5+}$ and Fe^{4+} centers with oxygen and chloride ligands (in total 30 Fe sites, geometry-optimized with COSMO with methanol as solvent) gave r^2 = 0.867, α = −0.307, and C = 0.385.[14]

The fit parameters listed in Table 3 were used to predict isomer shifts of the compounds included in the universal fit (Table 4). The mean absolute error of the predicted isomer shifts is 0.040 and 0.039 mms^{-1} for the gas-phase and solvent fits, respectively. The maximum absolute error is observed for $[Fe(SEt)_4]^-$, which is 0.12 mms^{-1} in both the gas phase and in the solvent (Table 4).

We also prepared an isomer shift fit involving only the NO complexes (Figure 6). Both the gas-phase and solvent-based FeNO fits have slightly improved parameters, relative to the universal fit (Table 3). Thus, the mean absolute error for predicted isomer shifts of all complexes included in the FeNO fit is 0.029 mms^{-1} in the solvent and 0.027 mms^{-1} in the gas phase. The maximum error was observed for $[Fe(H_2O)_5NO]^{2+}$, whose predicted isomer shift has an absolute error of 0.079 mms^{-1} in the solvent and 0.035 mms^{-1} in the gas phase.

(e) Mössbauer Parameters of Roussin's Black Salt

The fits described above were used to predict the isomer shifts of Roussin's black salt (RBS), $[Fe_4(NO)_7(\mu_3\text{-}S)_3]^-$, based on computed Fe nuclear densities for the apical $\{FeNO\}^7$ and the basal $\{Fe(NO)_2\}^9$ units. The molecule has C_{3v} symmetry, i.e. all basal irons are equivalent. Two different isomer shifts are thus expected, one for the $\{FeNO\}^7$ unit and one for the $\{Fe(NO)_2\}^9$ units (Table 5). It is important to keep in mind the constraints imposed on interpreting the experimental Mössbauer spectrum, when comparing the predicted isomer shifts to experimental values. Assuming that all four iron sites are equivalent gives an experimental isomer shift of 0.157 mms^{-1} (78 K), while assuming two different sites in a 3:1 ratio gives isomer shifts of 0.127 and 0.243 mms^{-1} (78 K) for the basal and apical irons, respectively.[63] We have used the latter results here, for comparing with our theoretically derived values. Correcting the experimental values to 4.2 K gives δ's of 0.16 and 0.27 and mms^{-1} for the two types of iron centers, respectively. The predicted isomer shifts reproduce the trend of the experimental values; however, the calculated difference between the two shifts is significantly lower than that observed experimentally (Table 5). While the predicted isomer shift of the basal $\{Fe(NO)_2\}^9$ irons (0.14 to 0.16 mms^{-1}) is very close to the experimental (temperature-corrected) value (0.16 mms^{-1}), the calculated result for the apical $\{FeNO\}^7$ iron is less accurate, with predicted isomer shifts of 0.17 to 0.19 mms^{-1}, compared to an experimental (temperature-corrected) value of 0.27 mms^{-1} (Table 5).

(f) Quadrupole splittings

The quadrupole splitting ΔE_Q results from the interaction between the electric quadrupole moment Q of the ^{57}Fe nucleus and the Electric Field Gradient (EFG) at the same nucleus. The asymmetric charge distribution around the Fe atom results in a splitting of the I = 3/2 ^{57}Fe nuclear excited state into $m_I = \pm 1/2$ and $m_I = \pm 3/2$. In a Mössbauer spectrum, this is observed as a splitting of the individual peaks into doublets, and the quadrupole splitting is measured as the distance between the doublet peaks. In the presence of a magnetic field, additional Zeeman splitting occurs, and the peaks split into sextets. Computationally, the quadrupole splitting may be determined by calculating the components of the electric field gradient (V) at the iron nucleus, V_{zz}, V_{yy}, and V_{xx}. After reordering to ensure that $|V_{zz}| \geq |V_{yy}| \geq |V_{xx}|$, the asymmetry parameter η is given by

$$\eta = |(V_{xx} - V_{yy})/V_{zz}|. \quad (4)$$

The quadrupole splitting is then calculated as

$$\Delta E_Q = \frac{1}{2} eQV_{zz} \sqrt{1 + \frac{\eta^2}{3}}, \quad (5)$$

where *e* is the electric charge of a positron and *Q* is the nuclear excited-state quadrupole moment. A value of 0.15 electron-barn was used for the nuclear quadrupole moment of ^{57}Fe. 71

Here we have computed the quadrupole splittings for all compounds listed in Table 1. For each electronically unique iron atom of a given structure (in the geometry-optimized broken symmetry state), the electric field gradient (*V*) at the iron nucleus was computed with ADF. The quadrupole splitting was then determined from the EFG tensor with the small utility code QUTIL, which calculates ΔE_Q according to equation (5). For polynuclear complexes with only one reported experimental quadrupole splitting, the calculated quadrupole splittings were averaged over iron centers that can be considered equivalent.

Quadrupole splittings may be either positive or negative. However, experimentally, the sign typically is not determined. Therefore, all experimentally determined quadrupole splittings are reported as absolute values. The sign of the computed quadrupole splitting is given in Table 6. When the asymmetry parameter η (equation 2) is close to 1, the sign of the quadrupole splitting is easily affected by the environment and a sign change may occur between the gas phase and solvent calculations.[a] This occurs for example for $[Fe(NO)_2\{Fe(NO)(NS_3)\}$-*S*, *S*′], which exhibits a sign change for the computed ΔE_Q for both iron centers in going from gas phase to solvent (Table 6).

The mean absolute errors are 0.28 mms^{-1} for both the gas-phase and COSMO ΔE_Q calculations, indicating that both approaches are equally good. However, for most complexes, the quadrupole splittings are underestimated compared to experimental values. Only for 4 out of 26 iron centers in Table 6 show a slight overestimation The maximum absolute error was observed for the mononuclear iron complex $[Fe(S_4C_8O_4)]^{2-}$, whose quadrupole splittings in the gas phase and in methanol are 0.71 and 0.75 mms^{-1} below the experimental value, respectively.

The OLYP quadrupole splittings of the nonheme iron nitrosyl complexes exhibit larger errors, relative to the nonnitrosyl complexes. Thus the mean absolute errors are 0.34 mms^{-1} (0.36 mms^{-1}) and 0.23 mms^{-1} (0.22 mms^{-1}), respectively, for the nitrosyl and nonnitrosyl complexes listed in Table 6 (gas phase values in parenthesis). Thus there appears to be a significant difference in error between the two sets of complexes. Several factors might contribute to the error in calculated quadrupole splittings. These include the temperature dependence of ΔE_Q, the magnitude of the ^{57}Fe nuclear quadrupole moment and the choice of the exchange-correlation functional.

The computed quadrupole splittings do not account for temperature corrections, i.e. they may be considered to correspond to the values at 0 Kelvin. Quadrupole splittings are temperature-dependent, but the dependence varies from complex to complex and no linear correction can be applied. The temperature dependence arises from geometric distortions due to temperature and from the population of low-lying excited states. Table 7 compiles experimentally

[a]This may be seen from the trace equation $V_{xx} + V_{yy} + V_{zz} = 0$. When η approaches 1, either V_{xx} or V_{yy} will be close to zero, whereas V_{zz} and the non-zero component (e.g. V_{yy}) will have similar magnitudes, but *opposite* signs. Given a small change in magnitude (due to a change of environment), V_{yy} might become slightly larger than V_{zz}. Now, according to convention, the EFG components are labeled based on magnitude; V_{yy} thus now becomes V_{zz}. The new V_{zz} will now have the opposite sign, thereby switching the sign of ΔE_Q (see equation 5).

determined quadrupole splittings at different temperatures for some of the compounds studied here. The mononuclear iron nitrosyl [Fe(NO)(dtc*i*-$Pr_2)_2$] and the tetramer complex [$Fe_4(NO)_4(\mu_3$-$S)_4$] have essentially the same quadrupole splittings at 300 K as at 4.2 K, whereas several of the Fe_4S_4 cluster complexes more than double their quadrupole splitting on lowering the temperature from 300 to 4.2 K (Table 7). The temperature dependence may be expected to constitute a key source of uncertainty in comparing the quadrupole splitting calculations with experiment, where low temperature experimental data is not available (Table 6).

The temperature dependent $|\Delta E_Q|$ data in Table 7 also shows, for the Fe_4S_4 cubane (nonnitrosyl) complexes, a much smaller difference between the DFT calculated quadrupole splittings and experiment at T = 4.2 K and 77 K than at 300 K. This result is surprising since the relevant thermal excitation energies are in all cases quite small (kT = 0.59, 0.15, and 0.01 kcal/mol at T = 300, 77, and 4 K) compared with expected electronic energy differences of about 10 kcal/mol or more for Fe d → d transitions in these systems. Electronic mixing must be sensitive to geometric distortions in these cubanes.

Another source of error lies in the nuclear quadrupole moment in equation (5). A value of 0.15 electron-barn was used for *eQ*;[71] however, a larger values of 0.2 electron-barn has also been reported for ^{57}Fe, based on earlier and less accurate data.[72] Careful quantum chemical calculations have suggested a value of 0.156 to 0.158 electron-barn.[73] If a value of 0.157 *eQ* is used here to compute quadrupole splittings, a slight reduction in error is observed, with a mean absolute error of 0.25 mms^{-1} for OLYP/COSMO-based quadrupole splittings.

Finally, pure functionals and hybrid functionals typically result in significantly different degrees of spatial separation of α and β spin densities in broken-symmetry calculations.[7,8,74,75] This might very well affect the computed EFG components and the quadrupole splittings. Here we have recomputed the quadrupole splittings for five complexes with B3LYP (using OLYP optimized geometries). Four of the five complexes, $[Fe(SEt)_4]^-$, $[Fe(S_4C_8O_4)]^{2-}$ and the two mononuclear {FeNO}^{7} complexes, exhibit nearly the same absolute quadrupole splitting with OLYP (Table 6) and with B3LYP (Table 8), although for $[Fe(S_4C_8O_4)]^{2-}$ the sign changes. The $[Fe(SPh)_4]^{2-}$ complex also experiences a sign change with the functional. For this complex, $|\Delta E_Q|$ is underestimated by 0.54 mms^{-1} with OLYP (Table 6), but overestimated by 0.13 mms^{-1} with B3LYP (Table 8). For a given complex, there might thus be significant differences between the two functionals. However, the mean absolute error for the five complexes (0.415 mms^{-1} with OLYP and 0.404 mms^{-1} with B3LYP) are comparable for the two functionals.

Conclusions

DFT (OLYP/STO-TZP) calculations on 9 nonheme iron nitrosyl complexes yield broken-symmetry states with significant spatial separation of α and β spin densities. Two isomer shift fits including these complexes were prepared, a universal fit also including 12 additional nonnitrosyl complexes (24 distinct iron sites) and an FeNO fit (10 distinct iron sites). The correlation between computed nuclear densities and experimental isomer shifts is good, with r^2 values in the range of 0.911 to 0.979, depending on the fit. In other words, DFT does performs comparably well for isomer shifts of nonheme iron nitrosyls and nonnitrosyl complexes.

The OLYP quadrupole splitting calculations of 26 distinct iron sites exhibit a mean absolute error of 0.28 mms^{-1}. These calculations appear to indicate a clear difference between the nitrosyl and nonnitrosyl results. Thus, whereas OLYP/COSMO calculations of quadrupole splittings for nonnitrosyl complexes alone exhibit a mean absolute error of 0.23 mms^{-1}, the iron nitrosyls exhibit a mean error of 0.34 mms^{-1}. Quadrupole splitting calculations (with

broken-symmetry DFT) thus appear to be less accurate for nonheme iron nitrosyl complexes, relative to iron complexes in general.

Supplementary Material

Refer to Web version on PubMed Central for supplementary material.

Acknowledgments

This work was supported by the Research Council of Norway, via a YFF grant to AG, and by NIH grant GM39914 to LN. We thank Wen-Ge Han for discussions and assistance.

References

1. McCleverty JA. Chem Rev 2004;104:403–418. [PubMed: 14871130]
2. Ghosh, A., editor. The Smallest Biomolecules: Diatomics and Their Interactions with Heme Proteins. Elsevier; 2008.
3. Butler, A.; Nicholson, R. Life, Death and Nitric Oxide. RSC; 2003.
4. Ignarro, L., editor. Nitric oxide: Biology and Pathobiology. Academic; 2000.
5. Rose MJ, Mascharak PK. Curr Opin Chem Biol 2008;12:238–244. [PubMed: 18355461]
6. For a review of DFT calculations on metalloporphyrin-NO complexes, see: Ghosh A. Acc Chem Res 2005;38:943–954. [PubMed: 16359166]
7. Conradie J, Quarless DA, Hsu HF, Harrop TC, Lippard SJ, Koch SA, Ghosh A. J Am Chem Soc 2007;129:10446–10456. [PubMed: 17685516]
8. Conradie J, Ghosh A. J Phys Chem B 2007;111:12621–12624. [PubMed: 17935317]
9. Hopmann KH, Conradie J, Ghosh A. J Phys Chem B 2009;113:10540–10547. [PubMed: 19719290]
10. Zhang Y, Oldfield E. J Phys Chem A 2003;107:4147–4150.
11. Ghosh, A.; Hopmann, KH.; Conradie, J. Electronic Structure Calculations: Transition Metal-NO Complexes. In: Solomon, EI.; Scott, RA.; King, RB., editors. Computational Inorganic and Bioinorganic Chemistry. UK: John Wiley & Sons, Ltd; 2009. p. 389-410.Chichester
12. Enemark JH, Feltham RD. Coord Chem Rev 1974;13:339–406.
13. Han WH, Liu T, Lovell T, Noodleman L. J Comput Chem 2006;27:1292–1306. [PubMed: 16786546]
14. Han WH, Noodleman L. Inorg Chim Acta 2008;361:973–986.
15. Nemykin VN, Kobayashi K, Chernii VY, Belsky VK. Eur J Inorg Chem 2001:733–743.
16. Zhang Y, Mao J, Oldfield E. J Am Chem Soc 2002;124:7829–7839. [PubMed: 12083937]
17. Havlin R, Godbout N, Salzmann R, Wojdelski M, Arnold W, Schulz CE, Oldfield E. J Am Chem Soc 1998;120:3144–315.
18. Grodzicki M, Flint H, Winkler H, Walker FA, Trautwein AX. J Phys Chem A 1997;101:4202–4207.
19. Zhang Y, Gossman W, Oldfield E. J Am Chem Soc 2003;125:16387–16396. [PubMed: 14692781]
20. Praneeth VKK, Neese F, Lehnert N. Inorg Chem 2005;44:2570–2572. [PubMed: 15819537]
21. Zhang Y, Oldfield E. J Am Chem Soc 2004;126:9494–9495. [PubMed: 15291525]
22. Li M, Bonnet D, Bill E, Neese F, Weyhermüller T, Blum N, Sellmann D, Wieghardt K. Inorg Chem 2002;41:3444–3456. [PubMed: 12079463]
23. García Serres R, Grapperhaus CA, Bothe E, Bill E, Weyhermüller T, Neese F, Wieghardt K. J Am Chem Soc 2004;126:5138–5153. [PubMed: 15099097]
24. Neese F. Inorg Chim Acta 2002;337:181–192.
25. Römelt M, Ye S, Neese F. Inorg Chem 2009;48:784–785. [PubMed: 19102678]
26. Handy NC, Cohen AJ. Mol Phys 2001;99:403–412.
27. Lee C, Yang W, Parr RG. Phys Rev B 1988;37:785–789.
28. (a) teVelde G, Bickelhaupt FM, van Gisbergen SJA, Fonseca Guerra C, Baerends EJ, Snijders JG, Ziegler T. J Comput Chem 2001;22:931–967. (b) Fonseca Guerra C, Snijders JG, te Velde G,

Baerends EJ. Theor Chem Acc 1998;99:391–403.(c) ADF2007.01. SCM, Vrije Universiteit; Amsterdam, The Netherlands: http://www.scm.com

29. a) Klamt A, Schüürmann G. J Chem Soc: Perkin Trans 1993;2:799–805. b) Klamt A. J Phys Chem 1995;99:2224–2235. c) Klamt A, Jones V. J Chem Phys 1996;105:9972–9981.
30. Schmitt EA, Noodleman L, Baerends EJ, Hendrickson DN. J Am Chem Soc 1992;114:6109–6119.
31. http://www.chemcraftprog.com
32. Liu, T.; Noodleman, L.; Case, DA. Program hyper. The Scripps Research Institute; La Jolla, CA: 2003.
33. a) Becke AD. Phys Rev A 1988;38:3098–3100. [PubMed: 9900728] b) Becke AD. J Chem Phys 1993;98:5648–5652. c) Stephens PJ, Devlin FJ, Chablowski CF, Frisch M. J Phys Chem 1994;98:11623–11627.
34. Neese F. J Phys Chem Solids 2004;65:781–785.
35. Version 2.6, revision 35. Developed by Neese, F. with contributions from (alphabetical order) Becker, U.; Ganiouchine, D.; Koßmann, S.; Petrenko, T.; Riplinger, C.; Wennmohs, F., see: http://www.thch.uni-bonn.de/tc/orca/.
36. Schaefer A, Horn H, Ahlrichs R. J Chem Phys 1992;97:2571–2577.
37. a) Laaksonen L. J Mol Graph 1992;10:33–34. [PubMed: 1504051] b) Bergman DL, Laaksonen L, Laaksonen A. J Mol Graph Model 1997;15:301–306. [PubMed: 9640561]
38. Mouesca JM, Chen JL, Noodleman L, Bashford D, Case DA. J Am Chem Soc 1994;116:11898–11914.
39. Soda T, Kitagawa Y, Onishi T, Takano Y, Shigeta Y, Nagao H, Yoshioka Y, Yamaguchi K. Chem Phys Lett 2000;319:223–230.
40. Maelia LE, Millar M, Koch SA. Inorg Chem 1992;31:4594–4600.
41. MacDonnell FM, Ruhlandt-Senge K, Ellison JJ, Holm RH, Power PP. Inorg Chem 1995;34:1815–1822.
42. Coucouvanis D, Swenson D, Baenziger NC, Murphy C, Holah DG, Sfarnas N, Simopoulos A, Kostikas A. J Am Chem Soc 1981;103:3350–3362.
43. Mayerle JJ, Denmark SE, DePaphilis BV, Ibers JA, Holm RH. J Am Chem Soc 1975;97:1032–1045.
44. Gillum WO, Frankel RB, Foner S, Holm RH. Inorganic Chemistry 1976;15:1095–1100.
45. Salifoglou A, Simopoulos A, Kostikas A, Dunham RW, Kanatzidis MG, Coucouvanis D. Inorg Chem 1988;27:3394–3406.
46. Dunham WR, Bearden AJ, Salmeen IT, Palmer G, Sands RH, Orme-Johnson WH, Beinert H. Biochim Biophys Acta 1971;253:134–52. [PubMed: 4331269]
47. Ferraro DJ, Gakhar L, Ramaswamy S. Biochem Biophys Res Commun 2005;338:175–190. [PubMed: 16168954]
48. Excoffon P, Laugier J, Lamotte B. Inorg Chem 1991;30:3075–3081.
49. Cleland WE, Holtman DA, Sabat M, Ibers JA, DeFotis GC, Averill BA. J Am Chem Soc 1983;105:6021–6031.
50. Segal BM, Hoveyda HR, Holm RH. Inorg Chem 1998;37:3440–3443.
51. Kanatzidis MG, Baenziger NC, Coucouvanis D, Simopoulos A, Kostikas A. J Am Chem Soc 1984;106:4500–4511.
52. Silver J, Fern GR, Miller JR, McCammon CA, Evans DJ, Leigh GJ. Inorg Chem 1999;38:4256–4261.
53. Wanat A, Schneppensieper T, Stochel G, van Eldik R, Bill E, Wieghardt K. Inorg Chem 2002;41:4–10. [PubMed: 11782137]
54. Butcher RJ, Sinn E. Inorg Chem 1980;19:3622–3626.
55. Johnsson CE, Rickards R, Hill HAO. J Chem Phys 1969;50:2594–2597.
56. Sanina NA, Rakova OA, Aldoshin SM, Shilov GV, Shulga YM, Kulikov AV, Ovanesyan NS. Mendeleev Comm 2004;14:7–8.
57. Sanina NA, Aldoshin SM. Russ Chem Bull, Int Ed 2004;53:2428–2448.
58. Harrop TC, Tonzetich ZJ, Reisner E, Lippard SJ. J Am Chem Soc 2008;130:15602–15610. [PubMed: 18939795]
59. Feig AL, Bautista MT, Lippard SJ. Inorg Chem 1996;35:6892–6898. [PubMed: 11666858]

60. Davies SC, Evans DJ, Hughes DL, Konkol M, Richards RL, Sanders JR, Sobota P. J Chem Soc, Dalton Trans 2002:2473–2482.
61. Jaworska M. Polyhedron 2007;26:3247–3254.
62. Baird P, Bandy JA, Green MLH, Hamnett A, Marseglia E, Obertelli DS, Prout K, Qin J. J Chem Soc Dalton Trans 1991:2377–2393.
63. Sedney D, Reiff WM. Inorg Chim Acta 1979;34:231–236.
64. Chu CTW, Lo FYK, Dahl LF. J Am Chem Soc 1982;104:3409–3422.
65. D'Addario S, Demartin F, Grossi L, Iapalucci MC, Laschi F, Longoni G, Zanello P. Inorg Chem 1993;32:1153–1160.
66. Jaworska M, Stasicka Z. J Molec Struct 2006;785:68–75.
67. Gütlich, P.; Ensling, J. Inorganic Electronic Structure and Spectroscopy. In: Solomon, EI.; Lever, ABP., editors. Methodology. Vol. I. John Wiley & Sons, Inc.; New York: 1999. p. 161-211.
68. A similar intermediate-spin Fe^{3+} description was also proposed for the S = 1/2 state of Fe(salen)(NO), which is an S =1/2, 3/2 spin-crossover complex.[7]
69. Sinnecker S, Neese F, Noodleman L, Lubitz W. J Am Chem Soc 2004;126:2613–2622. [PubMed: 14982471]
70. Ghosh P, Bill E, Weyhermüller T, Neese F, Wieghardt K. J Am Chem Soc 2003;125:1293–1308. [PubMed: 12553831]
71. Martínez-Pinedo G, Schwerdtfeger P, Caurier E, Langanke K, Nazarewicz W, Söhnel T. Phys Rev Lett 2001;87:1–4.062701
72. Gütlich, P.; Link, R.; Trautwein, A. Mössbauer Spectroscopy and Transition Metal Chemistry. Vol. 3. Springer-Verlag; Berlin: 1978.
73. Sinnecker S, Slep LD, Bill E, Neese F. Inorg Chem 2005;44:2245–2254. [PubMed: 15792459]
74. Ghosh A. J Biol Inorg Chem 2006;11:712–724. [PubMed: 16841211]
75. Although numerous papers have examined the performance of DFT in more general ways, comparatively few have focused on the issue of antiferromagnetic coupling. See e.g. Valero R, Costa R, Moreira IDPR, Truhlar DG, Illas F. J Chem Phys 2008;128Art no. 114103

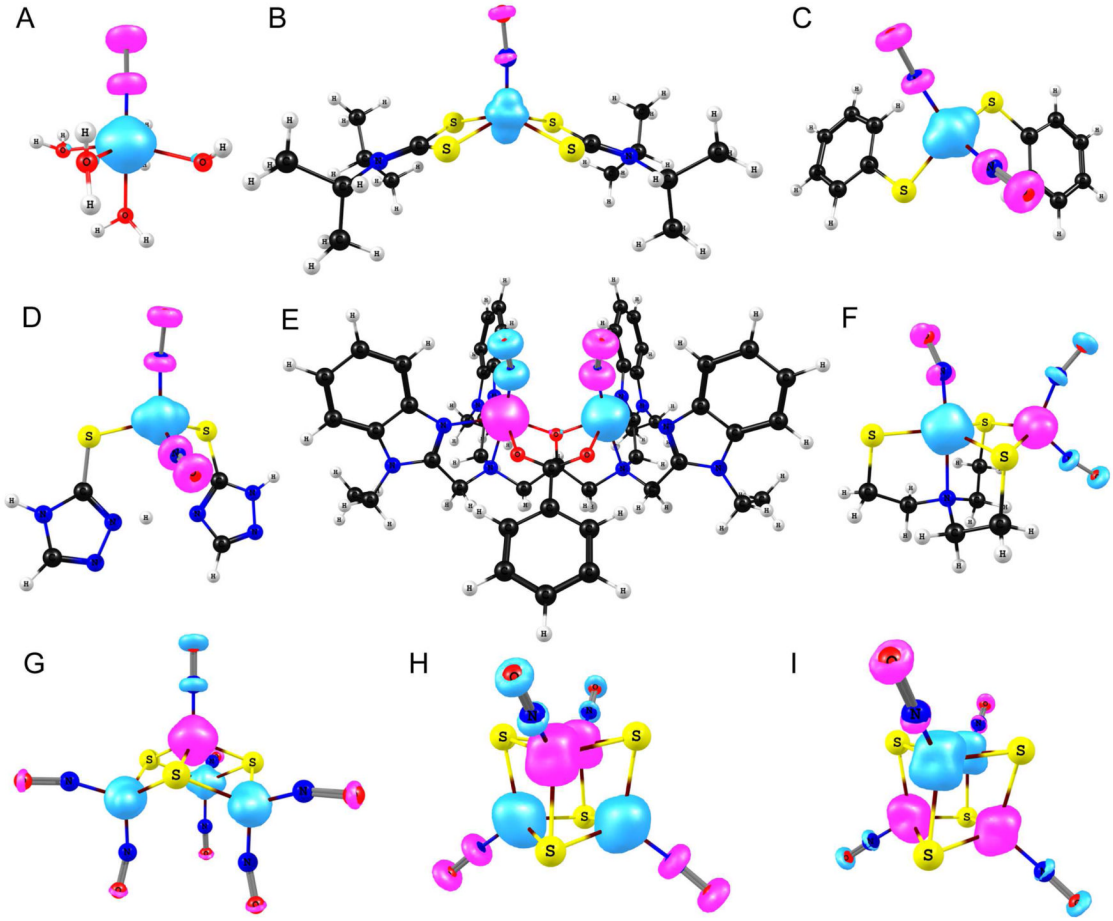

Figure 1.

OLYP spin densities for broken-symmetry states of iron nitrosyls: **A**, $[Fe(H_2O)_5(NO)]^{2+}$; **B**, $[Fe(NO)(dtc\textit{i}\text{-}Pr_2)_2]$; **C**, $[Fe(SPh)_2(NO)_2]^{-}$; **D**, $[Fe(SC_2H_3N_3)(SC_2H_2N_3)(NO)_2]$; **E**, $[Fe_2(NO)_2(Et\text{-}HPTB)(O_2CPh)]^{2+}$; **F**, $[Fe(NO)_2\{Fe(NO)(N(CH_2CH_2S)_3)\}$-*S*, *S*′]; **G**, $[Fe_4(NO)_7(\mu_3\text{-}S)_3]^{-}$; **H**, $[Fe_4(NO)_4(\mu_3\text{-}S)_4]^{-}$; **I**, $[Fe_4(NO)_4(\mu_3\text{-}S)_4)]$.

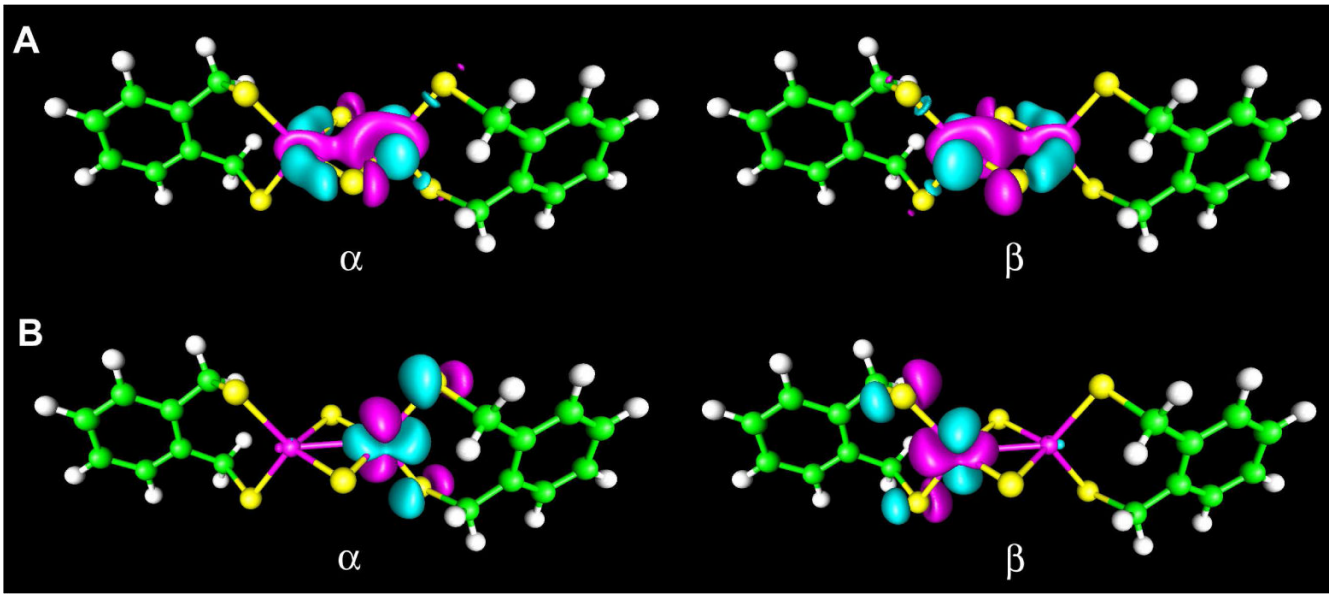

Figure 2.
Two of the five magnetic orbital pairs in $[Fe_2S_2(S_2\text{-o-xyl})_2]^{2-}$. The overlap values are 0.465 for A and 0.051 for B (contour value of 0.035, B3LYP, ORCA).

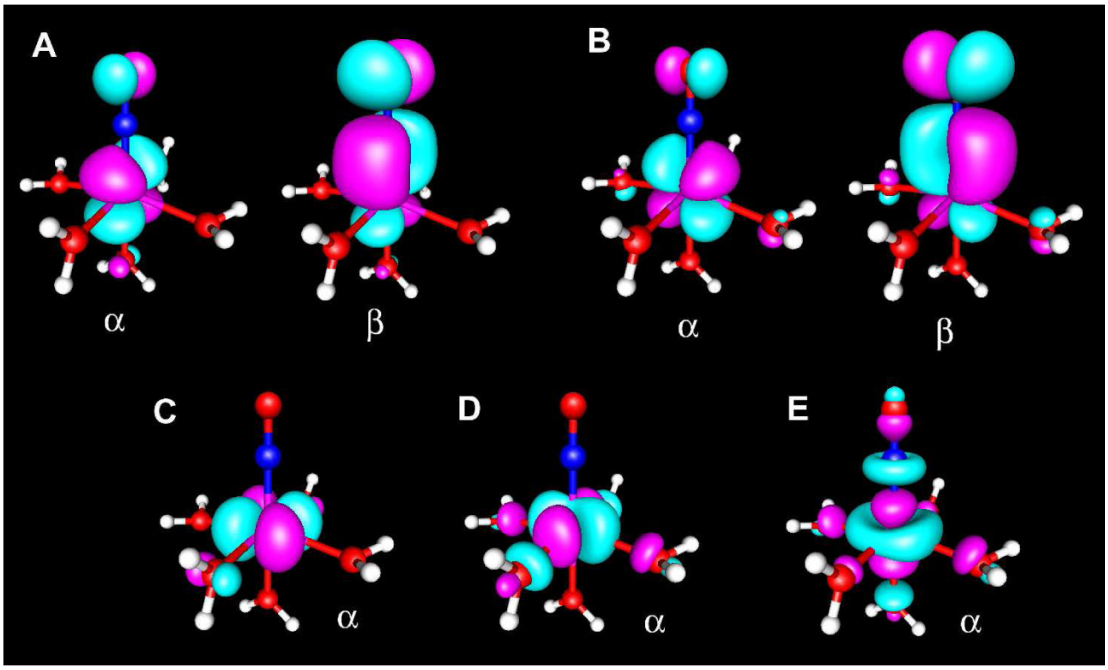

Figure 3.
Magnetic orbitals in $[Fe(H_2O)_5NO]^{2+}$. Orbital pairs with overlap A) 0.797 and B) 0.786 and SOMO orbitals C)-E) (contour value of 0.035, B3LYP, ORCA).

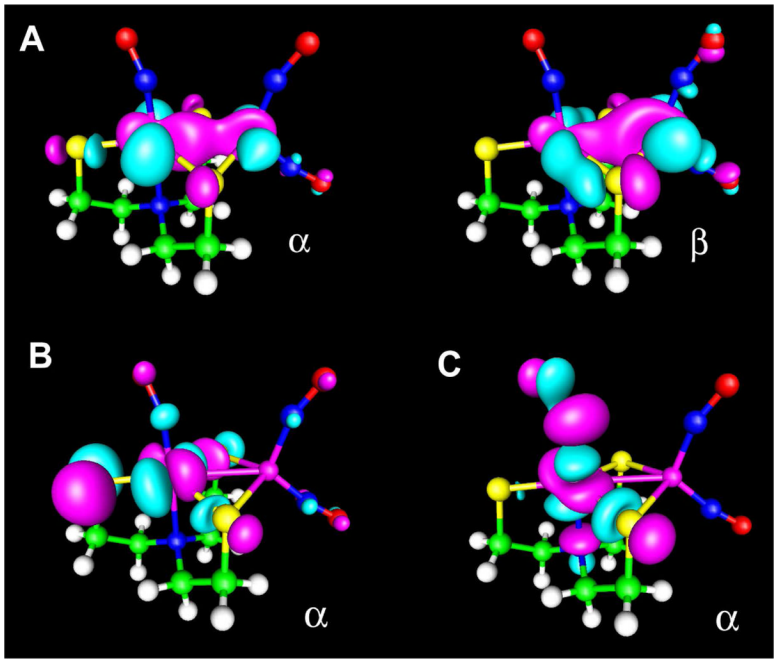

Figure 4.
Selected UCO (OLYP, ORCA, contour value 0.035) analysis results for $[Fe(NO)_2\{Fe(NO)(NS_3)\}$-*S*, *S*′]: A is a magnetic orbital pair (overlap 0.662) whereas B and C are SOMOs.

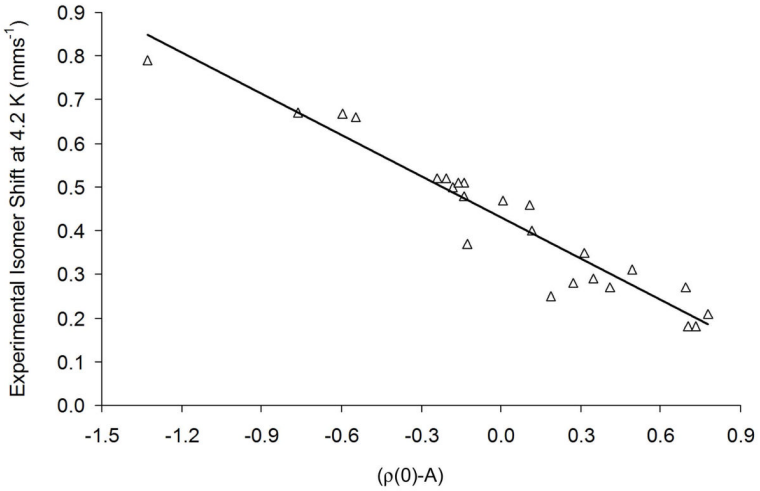

Figure 5.
Universal isomer shift fit based on 8 iron-NO complexes and 12 iron-sulfur complexes (24 distinct iron sites, ADF, OLYP/TZP, COSMO).

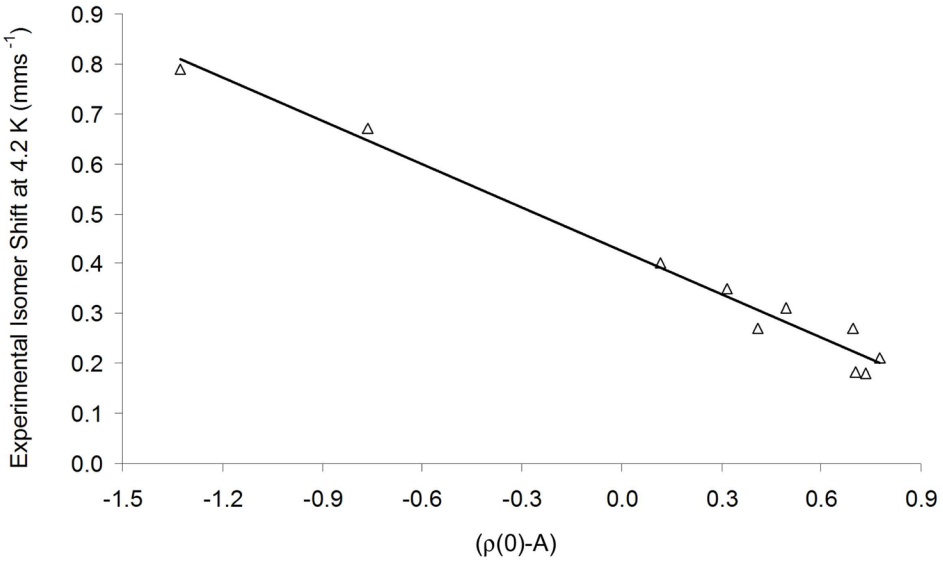

Figure 6.
FeNO isomer shift fit based on 8 iron nitrosyl complexes (10 distinct iron sites, ADF, OLYP/TZP, COSMO optimization).

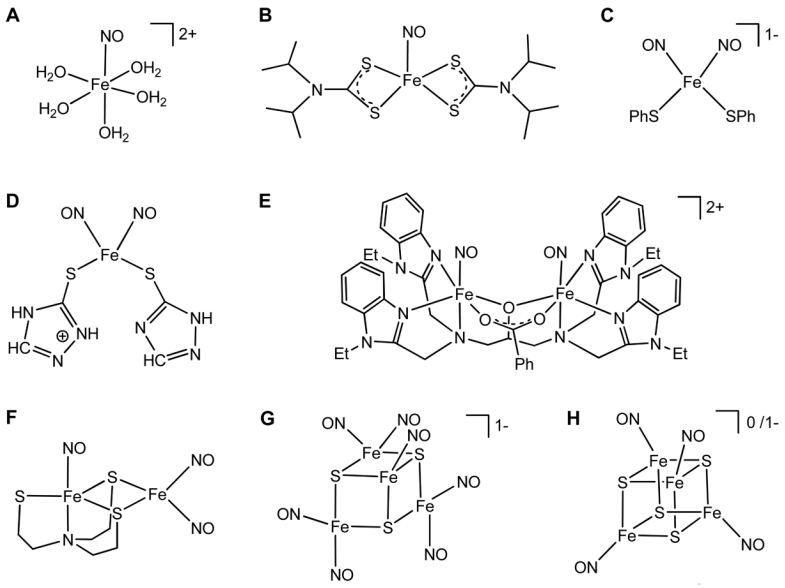

Scheme 1.

Iron nitrosyls included in this study: **A**, $[Fe(H_2O)_5(NO)]^{2+}$; **B**, $[Fe(NO)(dtc\textit{i}\text{-}Pr_2)_2]$ (dtc = dithiocarbamate); **C**, $[Fe(SPh)_2(NO)_2]^{-}$; **D**, $[Fe(SC_2H_3N_3)(SC_2H_2N_3)(NO)_2]$; **E**, $[Fe_2(NO)_2(Et\text{-}HPTB)(O_2CPh)]^{2+}$ (Et-HPTB = *N*, *N*, *N*′, *N*′-tetrakis-(*N*-ethyl-2-benzimidazolylmethyl)-2-hydroxy-1,3-diaminopropane); **F**, $[Fe(NO)_2\{Fe(NO)(N(CH_2CH_2S)_3)\}$-*S*, *S*′]; **G**, $[Fe_4(NO)_7(\mu_3\text{-}S)_3]^{-}$; **H**, $[Fe_4(NO)_4(\mu_3\text{-}S)_4]$ and $[Fe_4(NO)_4(\mu_3\text{-}S)_4]^{-}$.

Table 1

Iron complexes studied with DFT(OLYP/STO-TZP) calculations.

Complex	Structure ref[a]	S	Pt. Gr.[b]	Fe oxidation state	Fe spin pop.[c]	Ref.[d]
$[Fe(SEt)_4]^-$	CANDAW1	5/2	C_1	Fe^{3+}	3.79	40,41
$[FeS_4C_8O_4]^{2-}$	PTSQFE10	2	C_1	Fe^{2+}	3.57	42
$[Fe(SPh)_4]^{2-}$	PTHPFE10	2	C_1	Fe^{2+}	3.45	42
$[Fe(H_2O)_5NO]^{2+}$	-	3/2	C_1	$\{FeNO\}^7$	3.55	53
$[Fe(NO)(dtci\text{-}Pr_2)_2]$[e]	PRCBFE	1/2	C_1	$\{FeNO\}^7$	1.32	54,55
$[Fe(SPh)_2(NO)_2]^-$	SI[58]	1/2	C_1	$\{Fe(NO)_2\}^9$	1.57	58
$[Fe(SC_2H_3N_3)(SC_2H_2N_3)(NO)_2]$	EYABOV	1/2	C_1	$\{Fe(NO)_2\}^9$	1.75	56,57
$[Fe_2S_2(S_2\text{-}o\text{-}xyl)_2]^{2-}$	XLDTSF	0	C_s	Fe^{3+} Fe^{3+}	3.50 −3.50	43,44,45
$[Fe_2S_2(OPh\text{-}p\text{-}CH_3)_4]^{2-}$	GIBCUP	0	C_s	Fe^{3+} Fe^{3+}	3.68 −3.68	45
$[Fe_2S_2(C_4H_4N)_4]^{2-}$	CONSED10	0	C_{2v}	Fe^{3+} Fe^{3+}	3.67 −3.67	45
$[Fe_2(NO)_2(Et\text{-}HPTB)(O_2CPh)]^{2+}$	SI[59]	0	C_1	$\{FeNO\}^7$ $\{FeNO\}^7$	3.47 −3.47	59
$[Fe(NO)_2\{Fe(NO)(N(CH_2CH_2S)_3)\}\text{-}S, S']$	SI[60]	1	C_1	$\{FeNO\}^7$ $\{Fe(NO)_2\}^9$	2.61 −1.31	60
$[Fe_4S_4(SPh)_4]^{2-}$	FEMJAI02	0	C_1	$Fe^{2.5+}$ $Fe^{2.5+}$ $Fe^{2.5+}$ $Fe^{2.5+}$	3.17 3.18 −3.17 −3.18	48,51
$[Fe_4S_4(OPh)_4]^{2-}$	CAPGAB	0	C_1	$Fe^{2.5+}$ $Fe^{2.5+}$ $Fe^{2.5+}$ $Fe^{2.5+}$	3.34 3.35 −3.36 −3.36	49
$[Fe_4S_4(SPh)_2Cl_2]^{2-}$	CIYKUQ	0	C_1	$Fe^{2.5+}$ $Fe^{2.5+}$ $Fe^{2.5+}$ $Fe^{2.5+}$	3.27 3.32 −3.27 −3.33	51
$[Fe_4S_4(OPh)_2Cl_2]^{2-}$	CIYLAX	0	C_1	$Fe^{2.5+}$ $Fe^{2.5+}$ $Fe^{2.5+}$ $Fe^{2.5+}$	3.34 3.35 −3.34 −3.34	51
$[Fe_4S_4Cl_4]^{2-}$	NUSROI	0	C_{2v}	$2*Fe^{2.5+}$ $2*Fe^{2.5+}$	3.33 −3.33	50,51
$[Fe_4S_4(SCH_2CO_2Et)_4]^{2-}$	CEQYAY	0	C_2	$2*Fe^{2.5+}$ $2*Fe^{2.5+}$	3.28 −3.28	52
$[Fe_4(NO)_4(\mu_3\text{-}S)_4]$	KOCBUZ	0	C_{2v}	$2*\{FeNO\}^7$ $2*\{FeNO\}^7$	1.22 −1.22	62,63
$[Fe_4(NO)_4(\mu_3\text{-}S)_4]^-$ [g]	BIBMOO	1/2	C_{2v}	$2*\{FeNO\}^{7.5}$ $2*\{FeNO\}^7$	1.94 −1.29	64
$[Fe_4(NO)_7(\mu_3\text{-}S)_3]^-$ [h]	LAHSIW	0	C_{3v}	$\{FeNO\}^7$ $3*\{Fe(NO)_2\}^9$	−1.18 0.62	63,65

[a] Cambridge ID or reference to cif file (SI = Supplementary Information).

[b] Point group symmetry used in the calculations.

[c] Mulliken spin population (OLYP/COSMO).

[d] References for crystal structures and Mössbauer parameters.

[e] dtc = dithiocarbamate.

[f] Et-HPTB = *N*, *N*, *N*′, *N*′-tetrakis-(*N*-ethyl-2-benzimidazolylmethyl)-2-hydroxy-1,3-diaminopropane.

[g] Oxidation state assignment depends on electronic state.

[h] Not included in the isomer shift fit.

Table 2

OLYP/COSMO spin populations for broken-symmetry states of iron nitrosyls.

Compound	FeNO center	Fe	N	O
$[Fe(H_2O)_5(NO)]^{2+}$	$\{FeNO\}^7$	3.55	−0.42	−0.39
$[Fe(NO)(dtci\text{-}Pr_2)_2]$	$\{FeNO\}^7$	1.32	−0.17	−0.14
$[Fe(SPh)_2(NO)_2]^{1-}$	$\{Fe(NO)_2\}^9$	1.57	−0.25/−0.25	−0.19/−0.19
$[Fe(SC_2H_3N_3)(SC_2H_2N_3)(NO)_2]$	$\{Fe(NO)_2\}^9$	1.75	−0.28/−0.28	−0.22/−0.22
$[Fe_2(NO)_2(Et\text{-}HPTB)(O_2CPh)]^{2+}$	$\{FeNO\}^7$	3.47	−0.51	−0.40
	$\{FeNO\}^7$	−3.47	0.51	0.40
$[Fe(NO)_2\{Fe(NO)(N(CH_2CH_2S)_3)\}\text{-}S, S']$	$\{FeNO\}^7$	2.61	−0.19	−0.19
	$\{Fe(NO)_2\}^9$	−1.31	0.21/0.22	0.17/0.16
$[Fe_4(NO)_4(\mu_3\text{-}S)_4]$	$2*\{FeNO\}^7$	1.22	−0.17	−0.13
	$2*\{FeNO\}^7$	−1.22	0.17	0.13
$[Fe_4(NO)_4(\mu_3\text{-}S)_4]^-$	$2*\{FeNO\}^{7.5}$	1.94	−0.30	−0.22
	$2*\{FeNO\}^7$	−1.29	0.19	0.14
$[Fe_4(NO)_7(\mu_3\text{-}S)_3]^-$	$\{FeNO\}^7$	−1.18	0.16	0.13
	$3*\{Fe(NO)_2\}^9$	0.62	−0.09/−0.10	−0.07/−0.07

Table 3

Fit parameters for universal and FeNO isomer shift fits.

	α	C	r^2	Mean absolute error (mms^{-1})[a]
Universal Fit (COSMO)	−0.315	0.432	0.915	0.039
Universal Fit (Gas phase)	−0.302	0.416	0.911	0.040
FeNO Fit, (COSMO)	−0.290	0.426	0.979	0.029
FeNO Fit (Gas phase)	−0.271	0.410	0.975	0.027

[a]Mean absolute error for predicted isomer shifts for all compounds included in the fit.

Table 4

Experimental and predicted isomer shifts for all iron complexes included in the isomer shift fit.

Complex	Iron oxid. state[a]	Exp.[b] T (K)	Exp.[b] δ (mms^{-1})	T-corr.[c] δ (mms^{-1})	Predicted[d] Gas-ph. δ (mms^{-1})	Predicted[d] COSMO δ (mms^{-1})
$[Fe(SEt)_4]^{1-}$	Fe^{3+}	4.2	0.25	0.25	0.37	0.37
$[FeS_4C_8O_4]^{2-}$	Fe^{2+}	4.2	0.668	0.668	0.60	0.62
$[Fe(SPh)_4]^{2-}$	Fe^{2+}	4.2	0.66	0.66	0.60	0.60
$[Fe(H_2O)_5(NO)]^{2+}$	$\{FeNO\}^7$	80	0.76	0.79	0.87	0.85
$[Fe(NO)(dtc\textit{i}\text{-}Pr_2)_2]$[e]	$\{FeNO\}^7$	4.2	0.35	0.35	0.34	0.33
$[Fe(SPh)_2(NO)_2]^{1-}$	$\{Fe(NO)_2\}^9$	4.2	0.182	0.182	0.21	0.21
$[Fe(SC_2H_3N_3)(SC_2H_2N_3)(NO)_2]$	$\{Fe(NO)_2\}^9$	296	0.188	0.31	0.27	0.28
$[Fe_2S_2(S_2\text{-}o\text{-}xyl)_2]^{2-}$	$2*Fe^{3+}$	4.2	0.28	0.28	0.36	0.35
$[Fe_2S_2(OPh\text{-}\textit{p}\text{-}CH_3)_4]^{2-}$	$2*Fe^{3+}$	4.2	0.37	0.37	0.46	0.47
$[Fe_2S_2(C_4H_4N)_4]^{2-}$	$2*Fe^{3+}$	77	0.26	0.29	0.33	0.32
$[Fe_2(NO)_2(Et\text{-}HPTB)(O_2CPh)]^{2+}$	$2*\{FeNO\}^7$	4.2	0.67	0.67	0.65	0.67
$[Fe(NO)_2\{Fe(NO)(N(CH_2CH_2S)_3)\}$-*S*, *S*′]	$\{FeNO\}^7$	77	0.18	0.21	0.19	0.19
	$\{Fe(NO)_2\}^9$	77	0.37	0.40	0.40	0.39
$[Fe_4S_4(SPh)_4]^{2-}$	$4*Fe^{2.5+}$	4.2	0.46	0.46	0.43	0.40
$[Fe_4S_4(OPh)_4]^{2-}$	$4*Fe^{2.5+}$	4.2	0.5	0.5	0.48	0.49
$[Fe_4S_4(SPh)_2Cl_2]^{2-}$[f]	$2*Fe^{2.5+}$-SPh	4.2	0.48	0.48	0.47	0.48
	$2*Fe^{2.5+}$-Cl	4.2	0.51	0.51	0.50	0.47
$[Fe_4S_4(OPh)_2Cl_2]^{2-}$[f]	$2*Fe^{2.5+}$-OPh	4.2	0.51	0.51	0.47	0.48
	$2*Fe^{2.5+}$-Cl	4.2	0.52	0.52	0.48	0.50
$[Fe_4S_4Cl_4]^{2-}$	$4*Fe^{2.5+}$	4.2	0.52	0.52	0.50	0.51
$[Fe_4S_4(SCH_2COOEt)_4]^{2-}$	$4*Fe^{2.5+}$	78	0.43	0.47	0.43	0.43
$[Fe_4(NO)_4(\mu_3\text{-}S)_4]$	$4*\{FeNO\}^7$	78	0.15	0.18	0.20	0.20
$[Fe_4(NO)_4(\mu_3\text{-}S)_4]^{-}$	$2*\{FeNO\}^{7.5}$	RT[g]	0.156	0.27	0.21	0.30
	$2*\{FeNO\}^7$	RT[g]	0.156	0.27	0.29	0.21
Mean absolute error	-	-	-	-	0.040	0.039

[a] FeNO oxidation states are given in the Enemark-Feltham notation. The numbers preceding the * indicate the number of equivalent iron sites.

[b] Experimental values (see Table 1 for references).

[c] Temperature-corrected isomer shift (to 4.2 K) based on second-order Doppler shift.

[d] Prediction based on the universal fit.

[e] Experimental isomer shifts from $Fe(NO)(dtcEt_2)_2$.

[f] Experimental values were assigned so that smaller isomer shift was assigned to higher nuclear density.

[g] RT = room temperature, assumed to be 298 K.

Table 5

Predicted (OLYP) and experimental isomer shifts (mms^{-1}) for $[Fe_4(NO)_7(\mu_3\text{-}S)_3]^-$ (RBS).

	$\{FeNO\}^7$ unit	$\{Fe(NO)_2\}^9$ unit
Universal Fit (Solvent)	0.18	0.15
Universal Fit (Gas phase)	0.17	0.14
FeNO Fit, (Solvent)	0.19	0.16
FeNO Fit (Gas phase)	0.19	0.16
Experimental[a]	0.27	0.16

[a] Corrected to 4.2 K. See Table 1 for references.

Table 6

Experimental and Computed Quadrupole Splittings (OLYP).

Complex	Iron center	Exp.[a] T (K)	Exp.[a] $\|\Delta E_Q\|$(mms^{-1})	Gas phase η	ΔE_Q (mms^{-1})	COSMO η	ΔE_Q(mms^{-1})
$[Fe(SEt)_4]^{1-}$	Fe^{3+}	4.2	0.620	0.12	−0.37	0.09	−0.29
$[FeS_4C_8O_4]^{2-}$	Fe^{2+}	4.2	3.97	0.39	3.26	0.26	3.22
$[Fe(SPh)_4]^{2-}$	Fe^{2+}	4.2	3.24	0.54	−2.73	0.58	−2.70
$[Fe(H_2O)_5NO]^{2+}$	$\{FeNO\}^7$	80	2.1	0.02	−2.44	0.07	−2.29
$[Fe(NO)(dtc\textit{i}\text{-}Pr_2)_2]$[b]	$\{FeNO\}^7$	4.2	0.890	0.28	0.63	0.30	0.68
$[Fe(SPh)_2(NO)_2]^{1-}$	$\{Fe(NO)_2\}^9$	4.2	0.692	0.32	−0.26	0.45	−0.25
$[Fe(SC_2H_3N_3)(SC_2H_2N_3)(NO)_2]$	$\{Fe(NO)_2\}^9$	296	1.118	0.77	0.68	0.99	0.59
$[Fe_2S_2(S_2\text{-o-xyl})_2]^{2-}$	$2*Fe^{3+}$	4.2	0.36	0.31	−0.37	0.18	−0.38
$[Fe_2S_2(OPh\text{-}p\text{-}CH_3)_4]^{2-}$	$2*Fe^{3+}$	4.2	0.32	0.43	0.43	0.95	0.32
$[Fe_2S_2(C_4H_4N)_4]^{2-}$	$2*Fe^{3+}$	77	0.49	0.87	0.34	0.85	0.39
$[Fe_2(NO)_2(Et\text{-}HPTB)(O_2CPh)]^{2+}$	$\{FeNO\}^7$	4.2	1.44	0.25	−1.19	0.28	−1.32
$[Fe(NO)_2\{Fe(NO)(N(CH_2CH_2S)_3)\}$-*S, S*′]	$\{FeNO\}^7$	77	1.04	0.88	−0.63	0.94	0.58
	$\{Fe(NO)_2\}^9$	77	1.15	0.87	0.83	0.88	−0.87
$[Fe_4S_4(SPh)_4]^{2-}$	$4*Fe^{2.5+}$	4.2	1.07	0.81	0.87[d]	0.92	1.11
$[Fe_4S_4(OPh)_4]^{2-}$	$4*Fe^{2.5+}$	4.2	1.21	0.17	1.01	0.27	0.97
$[Fe_4S_4(SPh)_2Cl_2]^{2-}$ [c]	$2*Fe^{2.5+}$-SPh	4.2	0.9	0.43	0.78	0.81	0.70
	$2*Fe^{2.5+}$-Cl	4.2	1.22	0.06	0.95	0.09	0.91
$[Fe_4S_4(OPh)_2Cl_2]^{2-}$ [c]	$2*Fe^{2.5+}$-OPh	4.2	1.01	0.28	0.99	0.44	0.88
	$2*Fe^{2.5+}$-Cl	4.2	1.28	0.04	1.03	0.07	1.07
$[Fe_4S_4Cl_4]^{2-}$	$4*Fe^{2.5+}$	4.2	1.09	0.15	0.99	0.09	0.96
$[Fe_4S_4(SCH_2COOEt)_4]^{2-}$	$4*Fe^{2.5+}$	78	0.81	0.67	0.68	0.96	0.65
$[Fe_4(NO)_4(\mu_3\text{-}S)_4]$	$4*\{FeNO\}^7$	78	1.473	0.12	−1.10	0.15	−1.09
$[Fe_4(NO)_4(\mu_3\text{-}S)_4]^{-}$ [e]	$2*\{FeNO\}^{7.5}$	RT	0.935	0.41	1.18	0.42	1.19
	$2*\{FeNO\}^7$	RT	0.935	0.13	−0.62	0.08	−0.64
$[Fe_4(NO)_7(\mu_3\text{-}S)_3]^{-}$	$\{FeNO\}^7$	78	0.802	0.00	−0.38	0.00	−0.38
	$3*\{Fe(NO)_2\}^9$	78	0.895	0.06	0.36	0.10	0.40
Mean Absolute Error[f]					0.28		0.28

[a] For references, see Table 1.

[b] Experimental data from $Fe(NO)(dtcEt_2)_2$.

[c] Assignment of experimental values based on assignment of isomer shifts, Table 4.

[d] BS state exhibits two positive and two negative ΔE_Q, therefore averaging is performed over the absolute value.

[e] Only one reported experimental value, but the two nonequivalent centers are compared individually.

[f] Mean absolute errors were computed based on absolute values of quadrupole splittings.

Table 7

Temperature Dependence of Quadrupole Splittings.[55,51,63]

Complex	Exp $\|\Delta E_Q\|$ (mms^{-1}) 300 K	77 K	4.2 K	Calc 0 K[e]
$[Fe(NO)(dtc\textit{i}\text{-}Pr_2)_2]$[a]	0.89	0.87	0.89	0.68
$[Fe_4S_4(SPh)_4]^{2-}$	0.63	0.93	1.07	1.11
$[Fe_4S_4Cl_4]^{2-}$	0.38	0.67	1.09	0.96
$[Fe_4S_4(SPh)_2Cl_2]^{2-}$ [b]	0.39	0.64	0.90	0.70
	0.60	0.96	1.22	0.91
$[Fe_4S_4(OPh_2)Cl_2]^{2-}$ [b]	-[c]	0.78	1.01	0.88
	-[c]	1.09	1.28	1.07
$[Fe_4(NO)_4(\mu_3\text{-}S)_4]$	1.448	1.473[d]	1.461	1.09
MAE[f]				
All	0.38	0.16	0.20	
Nonnitrosyl Cubanes	0.42	0.12	0.17	
Nitrosyl	0.28	0.28	0.29	

[a] Experimental data for $[Fe(NO)(dtcEt_2)_2]$.

[b] Two distinct iron sites were observed experimentally.

[c] Not determined.

[d] 78 K.

[e] COSMO calculated DFT results.

[f] MAE = Mean absolute error.

Table 8

B3LYP computed quadrupole splittings.[a]

Complex	Iron oxidation state	Spin Population			Exp.[b] T (K)	Exp. $\|\Delta E_Q\|$ (mms^{-1})	COSMO	
		Fe	N	O			η	ΔE_Q (mms^{-1})
$[Fe(SEt)_4]^-$	Fe^{3+}	3.87	-	-	4.2	0.620	0.11	−0.20
$[Fe(S_4C_8O_4)]^{2-}$	Fe^{2+}	3.67	-	-	4.2	3.97	0.96	−3.10
$[Fe(SPh)_4]^{2-}$	Fe^{2+}	3.65	-	-	4.2	3.24	0.75	3.37
$[Fe(H_2O)_5NO]^{2+}$	$\{FeNO\}^7$	3.75	−0.46	−0.48	80	2.1	0.11	−2.39
$[Fe(NO)(dtc\textit{i}\text{-}Pr_2)_2]$	$\{FeNO\}^7$	2.00	−0.38	−0.51	4.2	0.890	0.32	0.58

[a] B3LYP single point calculations based on OLYP geometries, using ADF.

[b] For references see Table 1.